RADIATION RESEARCH **198**, 28–39 (2022)
0033-7587/22 $15.00

DOI: 10.1667/RADE-21-00021.1

# Exposure to 5 cGy $^{28}$Si Particles Induces Long-Term Microglial Activation in the Striatum and Subventricular Zone and Concomitant Neurogenic Suppression

Son T. Ton,[a,1] Julia R. Laghi,[a] Shih-Yen Tsai,[a] Ashley A. Blackwell,[c] Natalie S. Adamczyk,[a] Jenna R. Osterlund Oltmanns,[c] Richard A. Britten,[d] Douglas G. Wallace,[c] Gwendolyn L. Kartje[a,b]

[a] *Research Service, Edward Hines Jr. VA Hospital, Hines, Illinois;* [b] *Department of Molecular Pharmacology and Neuroscience, Loyola University Chicago Health Sciences Division, Maywood, Illinois;* [c] *Department of Psychology, Northern Illinois University, DeKalb, Illinois;* [d] *Department of Radiation Oncology, Eastern Virginia Medical School, Norfolk, Virginia*

**Ton ST, Laghi JR, Tsai S-Y, Blackwell AA, Adamczyk NS, Osterlund Oltman JR, Britten RA, Wallace DG, Kartje GL. Exposure to 5 cGy $^{28}$Si Particles Induces Long-Term Microglial Activation in the Striatum and Subventricular Zone and Concomitant Neurogenic Suppression. Radiat Res. 198, 28–39 (2022).**

**The proposed mission to Mars will expose astronauts to space radiation that is known to adversely affect cognition and tasks that rely on fine sensorimotor function. Space radiation has also been shown to affect the microglial and neurogenic responses in the central nervous system (CNS). We recently reported that a low dose of 5 cGy 600 MeV/n $^{28}$Si results in impaired cognition and skilled motor behavior in adult rats. Since these tasks rely at least in part on the proper functioning of the striatum, we examined striatal microglial cells in these same subjects. Using morphometric analysis, we found that $^{28}$Si exposure increased activated microglial cells in the striatum. The majority of these striatal Iba1$^+$ microglia were ED1$^-$, indicating that they were in an alternatively activated state, where microglia do not have phagocytic activity but may be releasing cytokines that could negatively impact neuronal function. In the other areas studied, Iba1$^+$ microglial cells were increased in the subventricular zone (SVZ), but not in the dentate gyrus (DG). Additionally, we examined the relationship between the microglial response and neurogenesis. An analysis of new neurons in the DG revealed an increase in doublecortin-positive (DCX$^+$) hilar ectopic granule cells (hEGC) which correlated with Iba1$^+$ cells, suggesting that microglial cells contributed to this aberrant distribution which may adversely affect hippocampal function. Taken together, these results indicate that a single dose of $^{28}$Si radiation results in persistent cellular effects in the CNS that may impact astronauts both in the short and long-term following deep space missions.** 

[1] Address for correspondence: Son Ton, PhD, Edward Hines Jr VA Hospital, 5000 S 5th Avenue, Research Service 151, Hines, IL 60141; email: son.ton@va.gov.

## INTRODUCTION

Space radiation is a generic term used to describe a mixture of highly energetic charged ions, ranging from protons to Fe ions. Current estimates suggest that astronauts will be exposed to ~13 cGy of space radiation during each year of the mission to Mars (*1*). The structure of the spacecraft will offer a degree of shielding to the astronauts, reducing the space radiation dose and altering the galactic cosmic radiation (GCR) ion and energy spectrum from that seen in free space. The ''local-field'' spectrum (the space radiation spectrum that the internal organs of astronauts will receive within the spacecraft) calculated using the current spacecraft design specifications predicts that the majority of the physical and dose equivalent space radiation dose will arise from $Z < 15$ particles (*2*).

We have recently reported that low-dose exposure of 600 MeV/n $^{28}$Si ($Z = 14$) results in impaired performance in cognitive (*3*) and fine motor skill (*4*) tasks. These data suggest that exposure to space radiation may be impacting the functionality of the striatum, given its key role in regulating motor behavior (*5*), attention (*6*), self-grooming (*7*), instrumental learning (*8, 9*), and in human outcome-based learning/decision making (*10*).

The mechanistic basis for space-radiation-induced loss of functionality of the brain remains largely unknown, but exposure to 5 cGy of 600 MeV/n $^{28}$Si has been shown to alter homeostatic synaptic plasticity long-term depression in the prefrontal cortex (*3*). Space radiation induced changes in the neurotransmission properties of neurons within other parts of the brain have also been widely reported (*11–18*).

Historically, neurons have been the principal cell type investigated after exposure to space radiation for their critical role in cognition functions, such as recognition and memory, and emotional regulation, including depression and anxiety. However, glial cells have recently been found to constituently regulate the excitability of neurons under both physiological and pathological conditions (*19–23*). Increased glial activation (neuroinflammation) is now

accepted to be a major driving force that accelerates the pathogenesis of neurodegenerative diseases, including Alzheimer's disease, Parkinson's disease, and multiple sclerosis (*24–28*). Some studies suggest that increased microglia activity (as measured by CD68 and Iba-1 immunoreactivity) may be the underlying cause for radiation-induced loss of hippocampal-dependent cognition (*29-31*). While hippocampal-dependent cognition is important, exposure to space radiation affects several cognitive processes and behaviors that are more dependent on the medial prefrontal cortex (mPFC) and medial striatum (*32*). Although exposure to space radiation increases microglial activity within the mPFC (*29*), it is presently unclear whether microglia within the medial striatum are also activated by space radiation.

To date, radiation-induced activation of microglial has primarily been evaluated solely from a neuroinflammatory perspective. Although microglia function as immune cells in the central nervous system (CNS), they also play an important role in regulating synaptic plasticity, synapse number (*33, 34*), neurogenesis (*35–37*), and rewiring of neural circuits (*38–41*). Therefore, the reduced neurogenesis (*42*) and increased microglia activation observed after radiation exposure may be inter-related (*43*). Radiation exposure results in neural precursor-cell dysfunction (*44*), reducing neurogenesis but not the intrinsic capacity of stem cells to differentiate into mature neurons. These data suggest that the microenvironment surrounding the neural stem cells has become non-permissive for neurogenesis. The exact basis for the non-permissive environment for precursor proliferation and differentiation in the irradiated brain is unknown, but the persistent presence of microglial cells is likely to be an important factor (*35–37,43*).

While exposure to space radiation leads to persistent high levels of microglial activation, the functionality of the activated microglial cells may be aberrant. Exposure to space radiation (*45*) and X rays (*46*) has been reported to result in persistent changes in the phagocytic and immune responsiveness of microglia. Thus, it is important to determine whether space radiation leads to differences in the functionality of microglia, in addition to characterizing the number of immunoreactive cells. Therefore, the current study was designed to determine whether exposure to 5 cGy of 600 MeV/n $^{28}$Si resulted in morphological and functional changes in microglia within the striatum, subventricular zone (SVZ), and dentate gyrus (DG) of adult rats, and whether such changes were correlated with reduced neurogenesis.

## METHODS

### *Animals*

All procedures were approved by the Institutional Animal Care and Use Committees of Eastern Virginia Medical School (EVMS), Brookhaven National Laboratory (BNL), and Northern Illinois University (NIU).

Male (proven breeder) Wistar rats (Hla®(WI)CVF®; Hilltop Lab Animals Inc., Scottsdale, PA) were used in this study. Brain tissue sections encompassing the three regions of interest (ROI): striatum, SVZ and DG were recovered from five sham-irradiated rats and five rats exposed to 5 cGy of 600 MeV/n $^{28}$Si [delivered at a rate of 2–5 cGy/min in the NASA Space Radiation Laboratory (NSRL)]. Sham-rradited rats were placed in identical irradiation jigs that remained in the preparation room, while their counterparts were taken into the radiation vault at NSRL. The average age at the time of irradiation was ten months old. Approximately three months postirradiation, rats underwent attentional set-shifting (ATSET) behavioral testing at EVMS as previously described (*3*). Rats that exhibited high-ATSET performance were then transported to NIU and screened for string-pulling performance as previously described (*4*). Two additional rats that did not undergo ATSET testing were also used in this study. The brains of the rats were recovered for histological analysis ~ one week after completion of the string-pulling assessments (i.e., five months postirradiation).

### *Perfusion, Tissue Processing and Histology*

The average age of rats at time of perfusion was 15 months. Rats were injected with phenytoin/pentobarbital (390 mg/kg, i.p.) and transcardially perfused with 4% paraformaldehyde (PFA). Brains were processed as follows: post-fixed overnight (4°C in 4% PFA), cryoprotected (30% sucrose in PBS, pH 7.4) until brains sank, cryosectioned coronally at 40-μm thickness, stored at –20°C in ethylene glycol, and antigen retrieval applied (99–100°C, 10 mM sodium citrate, pH 6.0, 15 min). All incubation times and washes were performed identically as described in our previous publications (*47, 48*). Phosphate-buffered saline (PBS) (pH 7.4, 0.2% Tween-20, 5% normal goat serum) was used to dilute antibodies to the correct working concentrations (see Table 1). Primary antibodies were incubated overnight (4°C), and secondary antibodies were incubated at room temperature for 2 h. All sections were mounted on gelatin-subbed slides and cover slipped with either Fluoromount G or Permount mounting medias. All investigators were blinded to the radiation exposure status of the individual rats whose sole identifier was an alphanumeric code. Once the histological evaluation was completed, the codes were then revealed.

### *Stereology*

All stereological counting procedures were performed similarly to our lab's previously published protocols (*47, 48*). The following parameters were used: four sections/animal/ROI, 480 μm apart: dorsal DG (–2.0 to –4.8 mm relative to bregma); anterior SVZ (+2.0 to –0.8 mm relative to bregma). The SVZ and granule cell layer (GCL) were outlined by tracing (2.5× objective), and the sampling grid size (64 × 150 μm) and the dissector window size (25 × 25 μm) were used. Counting was performed under high magnification (40×/0.75 NA objective, MBF Bioscience Leica DM400B microscope) excluding upper and lower focal planes to avoid oversampling. Cell counting and analysis were performed using Stereo Investigator software version 9.0.

### *Confocal Imaging*

To identify cells expressing Ki67, DCX, Iba1 and ED1, tissue sections were examined on a Leica SPE confocal microscope (Leica Microsystems Inc., Buffalo Grove, IL). Using a 10× objective, representative equivalent areas of the SVZ and DG were identified from a series of stained sections. Subsequently a 63×/1.3NA oil immersion objective was used to confirm double labeling of cells. All image acquisition settings were kept constant and image stacks were imported into Leica Application Suite X and compressed to maximum intensity Z projections.

**TABLE 1**
**Antibodies Used for Immunofluorescence and Immunohistochemistry**

| Primary antibodies | Target/Antigen | Antigen species | Immunogen | Source | Dilution |
|---|---|---|---|---|---|
| Rabbit anti-doublecortin (DCX) polyclonal | Neuroblast microtubule associated protein | Synthetic | Peptide of human DCX | Cell signaling 4604S [RRID: AB 10693771] | 1:500 |
| Rabbit anti-Iba1 polyclonal | Macrophage/microglia calcium binding protein | Synthetic | Peptide of C-terminus of Iba1 | Wako 019-19741 [RRID: AB_839503] | 1:1,000 |
| Rabbit anti-Ki67 polyclonal | Proliferation marker protein Ki-67 | Synthetic | KI67 fusion protein Ag26266 | Proteintech 27309 [RRID: AB_2756525] | 1:1,000 |
| Mouse anti-rat CD68 monoclonal (ED1) | Rat ED1, cytoplasmic glycosylated protein | Synthetic | Rat spleen cells | Bio-Rad MCA341R [RRID: AB_2291300] | 1:500 |
| Secondary antibodies | | | | | |
| Goat anti-mouse (AlexaFluor 488) polyclonal | Mouse IgG | Mouse | Gamma immunoglobins heavy and light chains | ThermoFisher A11001 [RRID: AB_10566289] | 1:500 |
| Goat anti-mouse IgG2a (AlexaFluor 488) polyclonal | Mouse IgG2a | Mouse | IgG2a | ThermoFisher A21131 [RRID: AB_141618] | 1:500 |
| Goat anti-rabbit (AlexaFluor 568) polyclonal | Rabbit IgG | Rabbit | Gamma immunoglobins heavy and light chains | ThermoFisher A11036 [RRID: AB_143011] | 1:500 |

*Morphological Analysis of Microglia*

Established methods were followed for analyzing microglia cells using FIJI (an open-source image processing package based on ImageJ2) and its Sholl analysis plugin (Fig. 1). Image Z-stacks were processed in Leica Application Suite X, imported into FIJI, and were processed by maximum intensity Z projection (Fig. 1A). Images of Iba1$^+$ cells were thresholded, despeckled and a binary mask was applied (Fig. 1B). To generate the circularity index (CI) of each individual cell, the area and perimeter (considering both cell body and processes) was measured using the ''measure'' tool in FIJI (Fig. 1B). Circularity index was calculated using the formula CI = (4pi(area)/(perimeter)^2). The Sholl analysis was done using the default settings, Radius step size = automatic (''0.00''), enclosing radius cutoff = one intersection, Sholl Method =

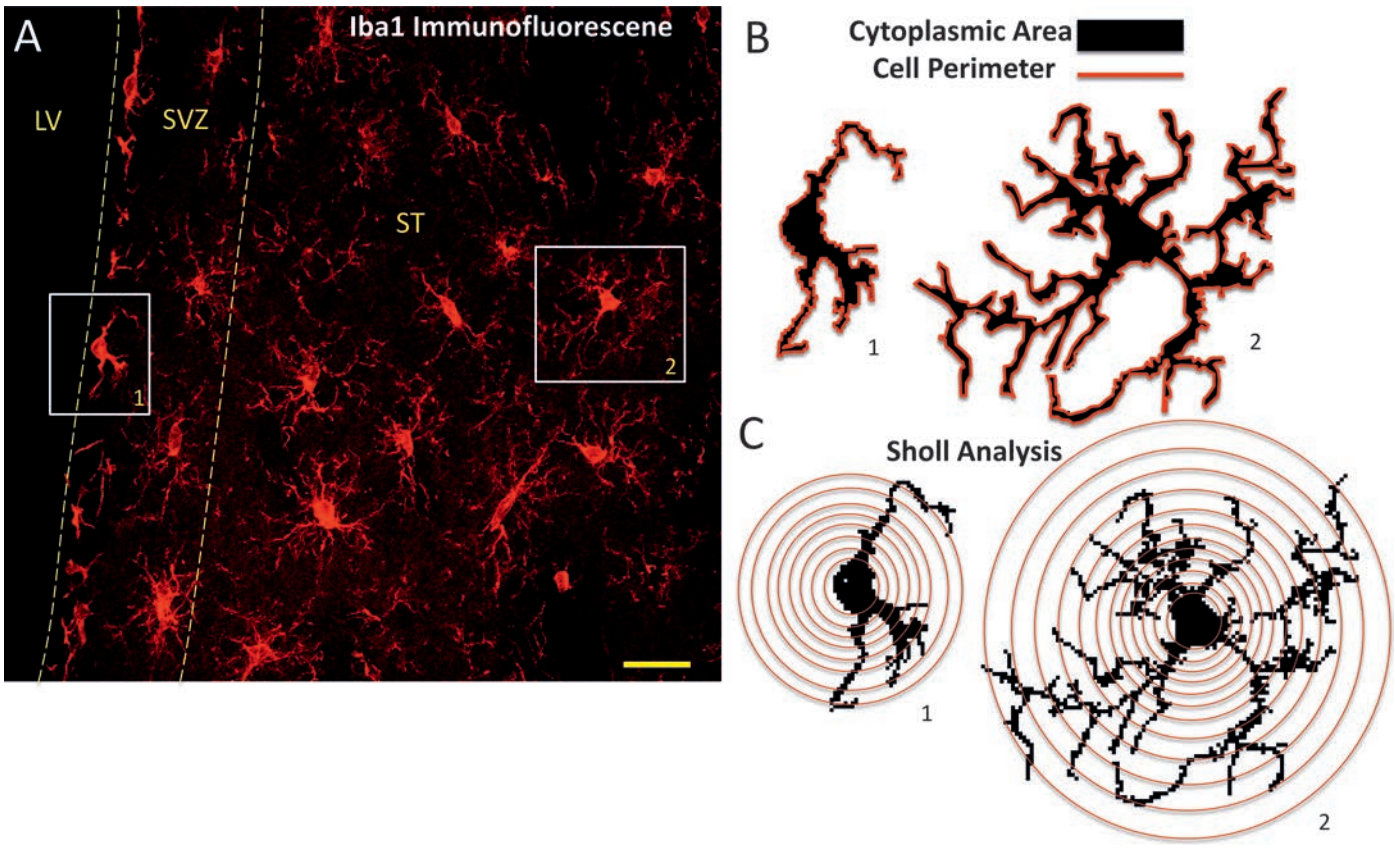


**FIG. 1.** Methods for analysis of microglia morphology. Panel A: A photomicrograph of Iba1$^+$ cells (red) captured from a confocal z-stack. White boxes enclose two example cells which were selected for analysis. Scale bar = 25 um. Panel B: Areas enclosed in white boxes in panel A were thresholded to obtain binary images. Microglial cytoplasmic area (black) and cell perimeter (red outlines) were measured for all complete cells within defined regions of interest. Panel C: Sholl analysis was performed to measure ramification index for up to 50 microglial cells per defined region of interest. ST = striatum; SVZ = subventricular zone; LV = lateral ventricle.

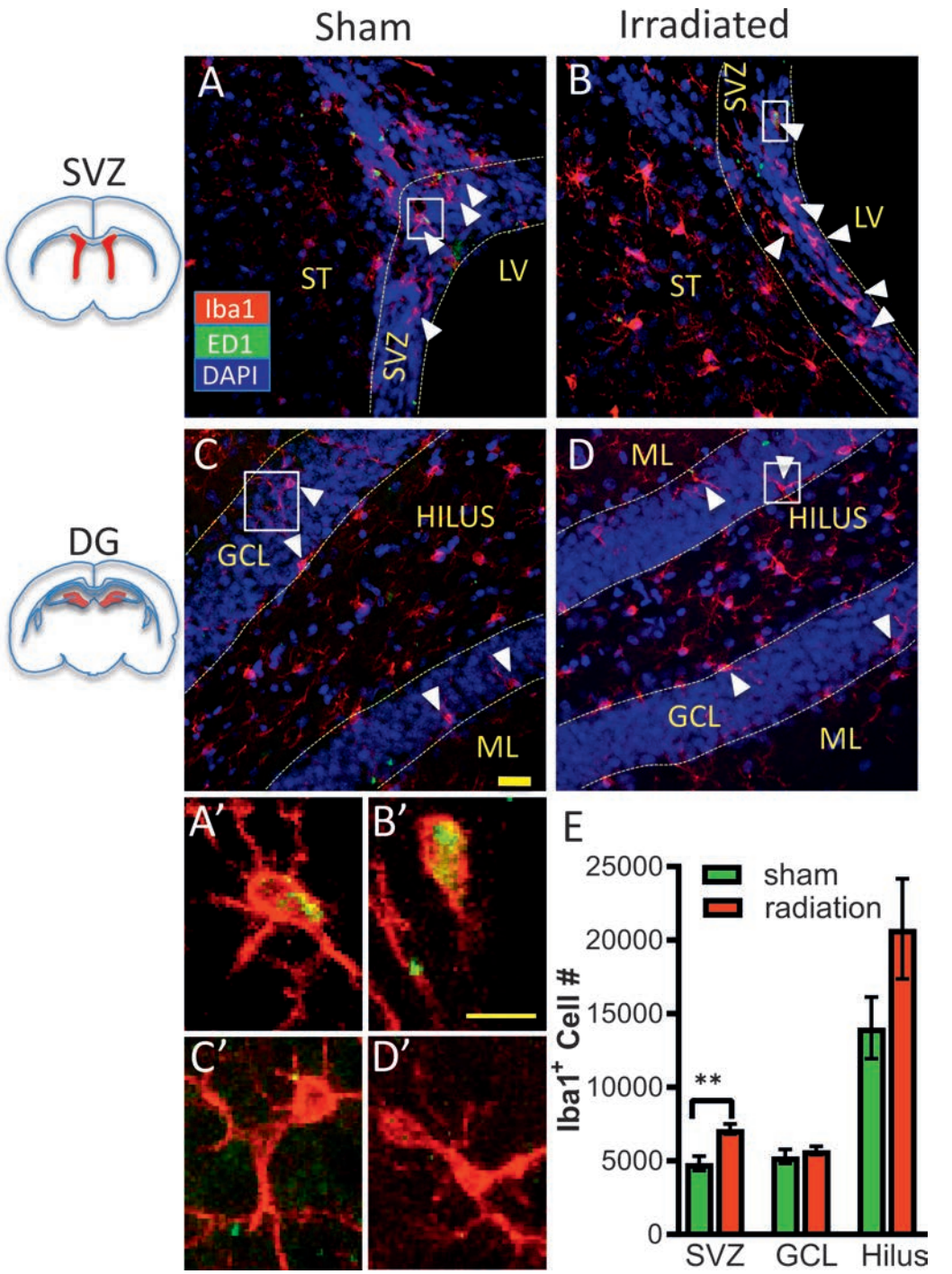


**FIG. 2.** [28]Silicon radiation increased microglia (Iba1$^+$) number in the subventricular zone but not the DG. Panels A–D: Representative immunofluorescence staining of the SVZ and DG showing distribution of Iba1$^+$(red), ED1$^+$(green) microglia cells, and DAPI$^+$ nuclei (blue). Yellow dashed lines outline the GCL and SVZ; arrowheads point to Iba1$^+$ cells. scale bar = 20 um. Panels A'-D' are enlargements of areas in white boxes in panels A–D, respectively, scale bar = 10 um. E. Histogram of Iba1$^+$ cell counts of SVZ, GCL and hilus. Student t test, **denotes $P \leq 0.005$, error bars = SEM. GCL = granule cell layer, ML = molecular layer, ST = striatum, LV = lateral ventricle.

linear. The Shoenen ramification index (RI) was calculated based on the number of end branches/number of primary branches for each cell (Fig. 1C). For each structure of interest (SVZ, medial striatum and DG), eight imaged regions encompassing both hemispheres were used. For each imaged region, all complete Iba1$^+$ cells were numbered, and six cells were randomly selected for analysis.

*Statistical analysis*

All data analysis was performed using Graphpad Prism version 9 (GraphPad Software, San Diego CA). All data were analyzed to determine normality of distribution, and non-normally distributed data were either analyzed using non-parametric tests or were transformed to

satisfy the normality and constant-variance requirements. Statistical methods, including data transformations (Box-Cox procedure) and Student t tests, were performed similar to previous work (*47, 48*).

## RESULTS

### *$^{28}$Si Exposure Increases Microglia Cells in the SVZ and Adjacent Striatum*

Iba1$^+$ signal was distributed throughout cell cytoplasm and labeled both the cell body and processes. The Iba1$^+$ cells exhibited a diverse morphology of shapes, ranging from round ameboid (activated state), to cells with highly branched processes (resting state). Iba1$^+$ microglial cells were present in both the SVZ and the adjacent striatum in all groups (Fig. 2A and B), but $^{28}$Si irradiation significantly increased the Iba1$^+$ cell count in the SVZ, [t(8) = 3.913, $P$ = 0.004] (Fig. 2E). Furthermore, there was a small but unique subpopulation of double-labeled Iba1$^+$/ED1$^+$ microglial cells (5% out of a total 708 SVZ Iba1$^+$ cells, 1% out of a total 1,080 striatal Iba1$^+$ cells) primarily located in the dorsal lateral aspect of the SVZ (Fig. 2A and B, Fig. 2A'and B').

Robust Iba1$^+$ staining was observed in all areas of the DG (Fig. 2C and D). $^{28}$Si exposure did not significantly change Iba1$^+$ microglia cell count in either the GCL or the hilus (Fig. 2E). Furthermore, no Iba1$^+$ /ED1$^+$ double labeled cells were observed in the DG (Fig. 2C' and D').

### *$^{28}$Si Exposure Increases Microglial Activation in the Medial Striatum and DG (when measuring morphological indices)*

In sham-irradiated rats, Iba1$^+$ microglia were morphologically distinct among the regions of interest (ROI: SVZ, medial striatum and DG hilus) (Supplementary Fig. S1A–D; https://doi.org/10.1667/RADE-21-00021.1.S1). There was a significant difference in cell area, perimeter, circularity, and ramification index for the three different ROIs ($P < 0.001$, one-way ANOVA, $n = 5$). Post hoc comparisons using the Tukey Honest Significant Difference (HSD) test were reported in Table 2.

Exposure to $^{28}$Si caused distinct changes in microglial morphology in the medial striatum and DG hilus, but not in the SVZ (Fig. 3A–D). In the striatum, $^{28}$Si exposure led to significant changes in microglial perimeter (median for sham = 236.8 μm; $^{28}$Si = 274.6 μm; Mann-Whitney U = 79897; $P = 0.020$), circularity (median for sham = 0.035; $^{28}$Si = 0.028; Mann-Whitney U = 24,164; $P = 0.013$), and ramification (median for sham = 1.333; $^{28}$Si = 1.250; Mann-Whitney U = 24,400; $P = 0.023$) indices. In the DG hilus, only microglial area (median for sham = 101.5 μm$^2$; $^{28}$Si = 93.84 μm$^2$; Mann-Whitney U = 185957; $P = 0.019$) was significantly different in the $^{28}$Si-irradiated rats.

Plots of circularity versus ramification indices revealed that microglia from $^{28}$Si-irradiated rats had less morphological variation compared to sham-irradiated rats, suggesting that space radiation led to a more activated microglial population (Fig. 4A–C and Supplementary Fig. S2; https://doi.org/10.1667/RADE-21-00021.1.S1).

**TABLE 2**
**Statistical Results**

| Antibody/Figure/Test | Data | Statistical results |
|---|---|---|
| Iba1 | SVZ | $t(8) = 3.913$, $P = 0.0045$ |
| Fig 2E | GCL | $t(7) = 0.6775$, $P = 0.5199$ |
| Student's t test | Hilus | $t(8) = 1.679$, $P = 0.1316$ |
| | Area | Hilus vs. SVZ:*** |
| | p<0.0001 | Hilus vs. Striatum:**** |
| | | SVZ vs. Striatum:* |
| Iba1 | Perimeter | Hilus vs. SVZ:**** |
| Supplementary Fig. S1 | $P < 0.0001$ | Hilus vs. Striatum:**** |
| One-way ANOVA | | SVZ vs. Striatum:**** |
| Tukey HSD post hoc | Circularity | Hilus vs. SVZ:**** |
| | $P < 0.0001$ | Hilus vs. Striatum:**** |
| | | SVZ vs. Striatum:* |
| | Ramification | Hilus vs. SVZ:** |
| | $P < 0.0001$ | |
| | | Hilus vs. Striatum:*** |
| | | SVZ vs. Striatum: ns |
| | | SVZ: ns |
| | Area | Striatum: ns |
| | | DG*, $P = 0.0190$ |
| | | SVZ: ns |
| | Perimeter | Striatum:*, $P = 0.0205$ |
| Iba1 | | DG: ns |
| Fig. 3 | | SVZ: ns |
| Mann-Whitney U test | Circularity | Striatum:*, $P = 0.0129$ |
| | | DG: ns |
| | | SVZ: ns |
| | Ramification | Striatum:*, $P = 0.0226$ |
| | | DG: ns |
| DCX | SVZ | ns, $t(7) = 2.562$, $P = 0.0773$ |
| Fig. 5 | GCL | ns, $t(8) = 2.288$, $P = 0.0514$ |
| Student's t test | Hilus | *, $t(8) = 2.973$, $P = 0.0178$ |
| Ki67, Fig. 7 | SVZ | *, $t(8) = 2.347$, $P = 0.0469$ |
| Student's t test | | |

### *$^{28}$Si Exposure Did Not Significantly Change Doublecortin Cells in the SVZ*

In the SVZ, DCX$^+$ immature neurons were also present in all rats (Fig. 5A and B, Fig. 5A' and B'). No significant effects of $^{28}$Si exposure were detected. However, there was a trend toward increased DCX$^+$ cell number in the irradiated group ($M = 593.4$, SEM = 68.45) compared to the sham group ($M = 448.0$, SEM = 32.39), $t(7) = 2.562$, $P = 0.077$ (Fig. 5E).

### *$^{28}$Si Exposure Increases Doublecortin Cells in the DG Hilus*

DCX$^+$ immature neurons were observed within the hilar region of the DG in $^{28}$Si-irradiated rats (Fig. 5C and D, Fig. 5C' and D'). $^{28}$Si exposure significantly increased hilar DCX$^+$ cell number as compared to sham-irradiated rats (Fig. 5E), [$t(8) = 2.973$, $P = 0.018$]. Furthermore, hilar DCX$^+$ cells exhibited atypical morphology with mostly round cell

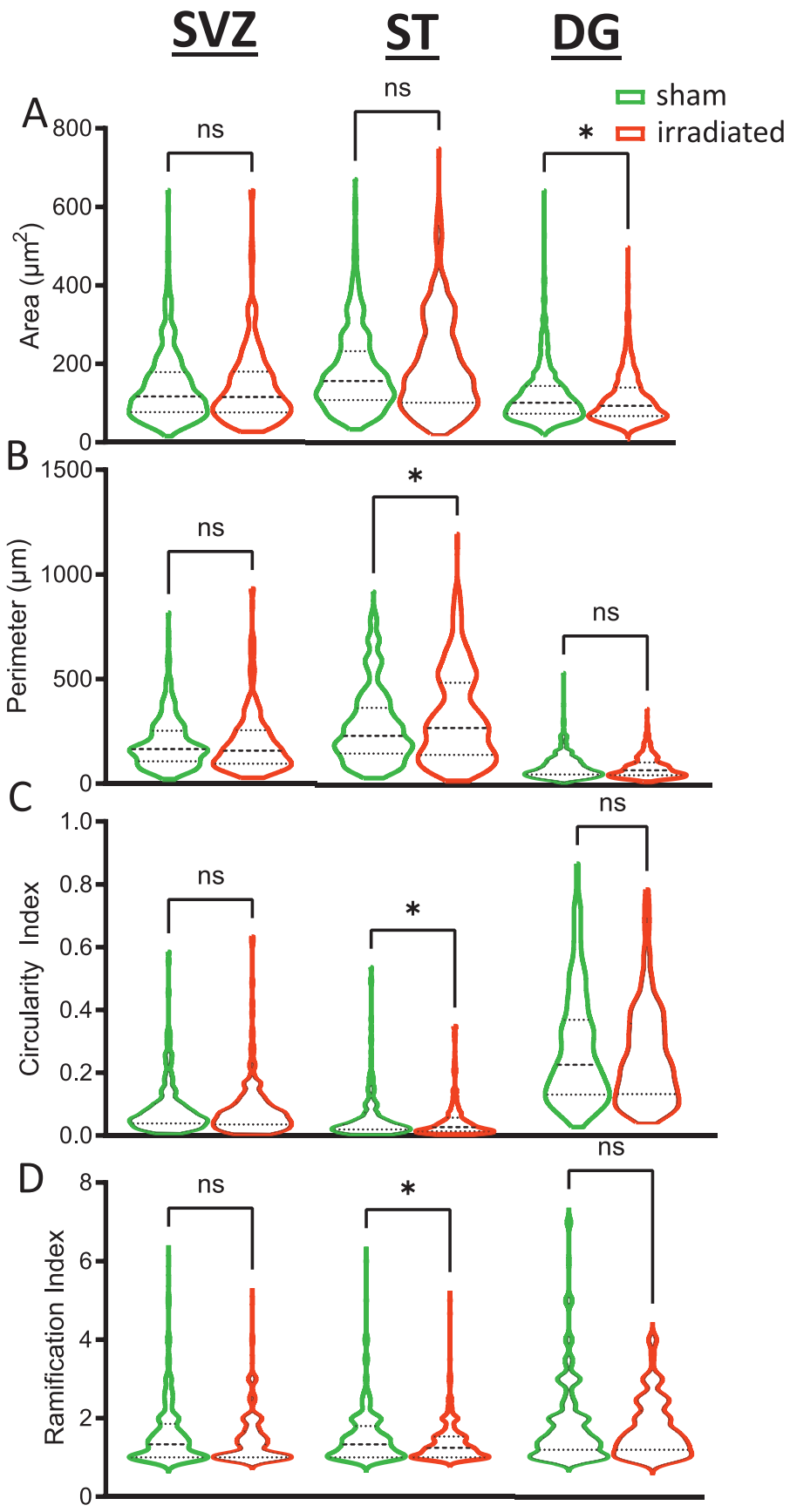


**FIG. 3.** [28]Silicon radiation changed microglia morphology in the striatum and DG. Violin plots of area (panel A), perimeter (panel B), circularity (panel C) and ramification (panel D) indexes. Dotted lines represent median, upper and lower quartiles. Mann-Whitney U tests, *denotes $P \leq 0.05$, ns = not significant.

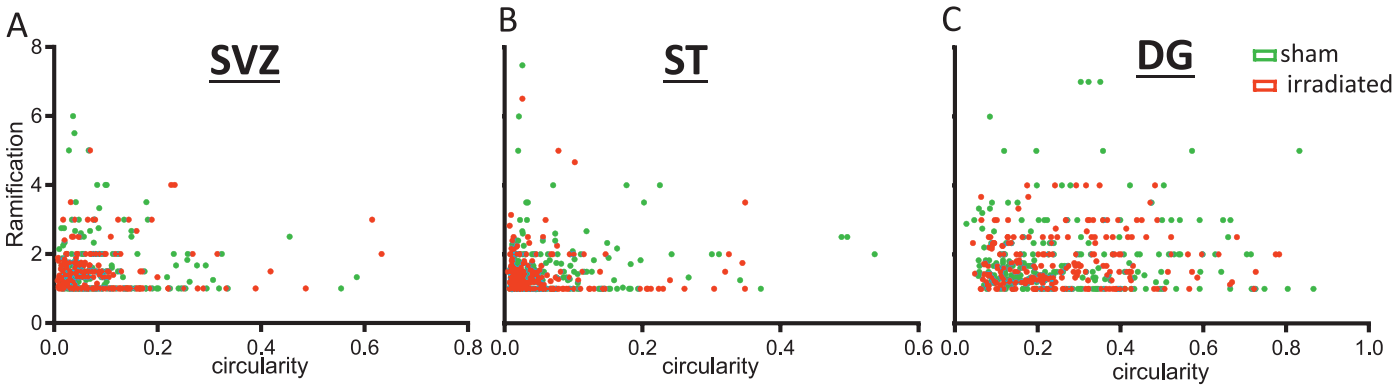


**FIG. 4.** $^{28}$Silicon radiation reduced the morphological heterogeneity in the SVZ, striatum and DG. Panels A–C. Scatter plots of circularity versus ramification. Each dot represents a single Iba1$^+$ cell.

bodies and few processes in contrast to the typical GCL DCX$^+$ cells that have fan-shaped dendritic trees extending toward the dentate molecular layer. However, no significant change in DCX$^+$ cell number was detected in the adjacent GCL, although there was a trend toward increased DCX$^+$ cell counts in the irradiated group (Fig. 5E), [$t(8) = 2.288$, $P = 0.051$].

### *Microglia and Immature Neurons were Positively Correlated in the SVZ and DG*

When combining both sham and irradiated groups, we detected a significant positive correlation between the number of microglial cells (Iba1$^+$) and immature neurons (DCX$^+$) in the SVZ [$r(8) = 0.653$, $P = 0.041$], and in the DG [$r(8) = 0.686$, $P = 0.028$] (Fig. 6A and B).

### *$^{28}$Si Exposure Reduces Proliferation in the SVZ, But Not in the DG*

Very few Ki67$^+$ cells were seen in the DG in both sham- and $^{28}$Si-irradiated groups, but those that were detected were also prospero homeobox protein 1 (Prox1$^+$), a transcription factor expressed in developing and mature granule cells (*49*) (figure not shown). In contrast to the DG, there was a robust presence of Ki67$^+$ proliferating cells in the SVZ in all rats, and some Ki67$^+$ cells were also seen in the adjacent striatum (Fig. 7A and B). Exposure to $^{28}$Si significantly reduced the number of Ki67$^+$ cells in the SVZ, [$t(8) = 2.347$, $P = 0.0469$] (Fig. 7C).

### *No Correlation between SVZ Microglial and Proliferating Cell Number*

There was no significant correlation between microglia (Iba1$^+$) cell number and proliferating (Ki67$^+$) cell number in the SVZ [$r(8) = -0.475$, $P = 0.165$] (Fig. 7D).

## DISCUSSION

The majority of studies to date which have characterized the impact that space radiation has on microglial activation have primarily been focused on the hippocampus. Some studies suggest that increased microglia activity may be the underlying cause for space radiation-induced loss of hippocampal-dependent cognition (*29–31, 43*). While hippocampal-dependent cognition is important, space radiation affects performance in several cognitive processes and behaviors that are more dependent on the mPFC and striatum (*32*). While exposure to space radiation does lead to increased microglial activity within the mPFC (*29*), it is presently unclear whether microglial activation within the striatum could underlie space radiation-induced changes in striatum-dependent behaviors, e.g., operant responses (*50–52*), social interactions (*30, 45, 53–56*), or fine motor skills (*4*).

In the current study, we found significant morphological difference in microglia among all the ROI examined. For instance, striatal microglia had larger soma sizes with long and thin processes, SVZ microglia had elongated shapes, while hilar microglia were small and highly ramified. These unique morphological differences may be a result of microglia adapting to the different microenvironments of the CNS. For instance, the elongated form of SVZ microglia may be due to their alignment with myelinated fibers present in this region. Remarkably, this microglia morphology is similar between rodents and humans (*57*). Importantly, we found significant changes to microglial morphology five months postirradiation, indicative of activation states in the medial striatum. These changes in morphology, notably, area and perimeter measurements, are two reliable morphological indices of microglia activation after brain trauma (*58*) and LPS-challenge (*59*). Moreover, cerebral ischemia results in a decreased ramification index of perilesional microglia and an increased accumulation of microglia in the peri-infarct striatum (*60, 61*). Thus, enhanced microglia activation may be one cellular mechanism underpinning space radiation-induced behavioral deficits (*4, 30, 43, 45, 50–56*). The importance of the elevated microglial activation within the medial striatum on fine motor skill performance is most direct, given that the rats used in the present study have documented impairments in string-pulling behavior (*4*). The majority of these striatal

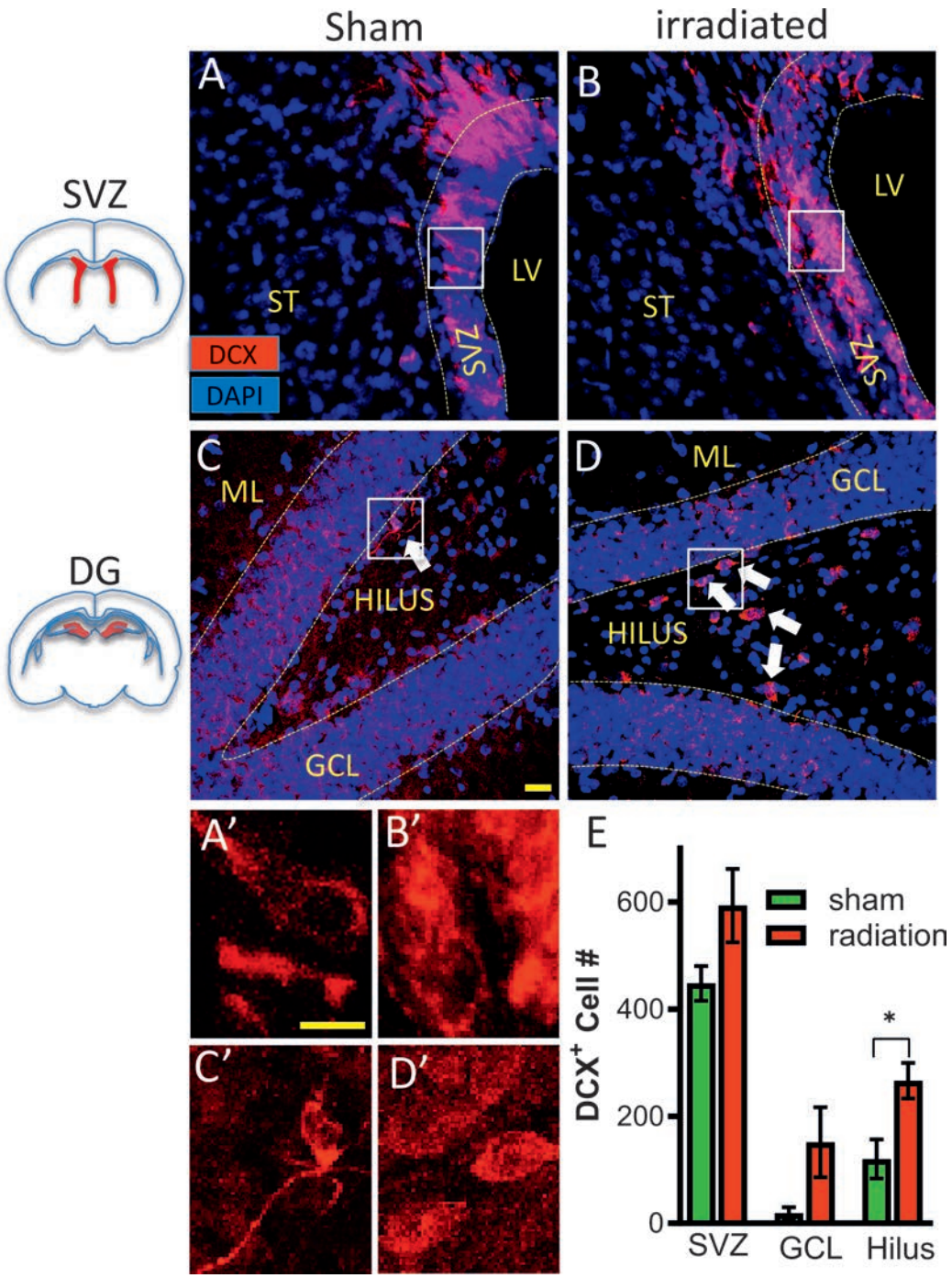


**FIG. 5.** [28]Silicon radiation increased dentate gyrus hilar newborn neurons ($DCX^+$) cells. Panels A–D: Representative DCX immunofluorescence staining of SVZ and DG showing robust DCX expression and elevated $DCX^+$ distribution in the hilus after [28]Si irradiation. Yellow dashed lines outline the GCL and SVZ; arrows point to $DCX^+$ cells. Scale bar = 20 μm. Panels A'-D' are enlargements of areas in white boxes in panels A–D, respectively, scale bar = 10 um. E. Histogram of $DCX^+$ cell count of SVZ, GCL and hilus. Student t test, *denotes $P \leq 0.05$, error bars = SEM. GCL = granule cell layer, ML = molecular layer, ST = striatum, LV = lateral ventricle.

$Iba1^+$ microglia were $ED1^-$ indicating that they may be in an alternatively activated state (*62*), where microglia do not have phagocytic activity but may be releasing cytokines that could negatively impact neuronal function. This long-term change to the CNS microenvironment in an area involving motor, motivation, attentional, and learning functions may have serious implications for astronauts during and after their deep space missions (*63*).

A central part of this study was the characterization of microglial numbers and activation status within the

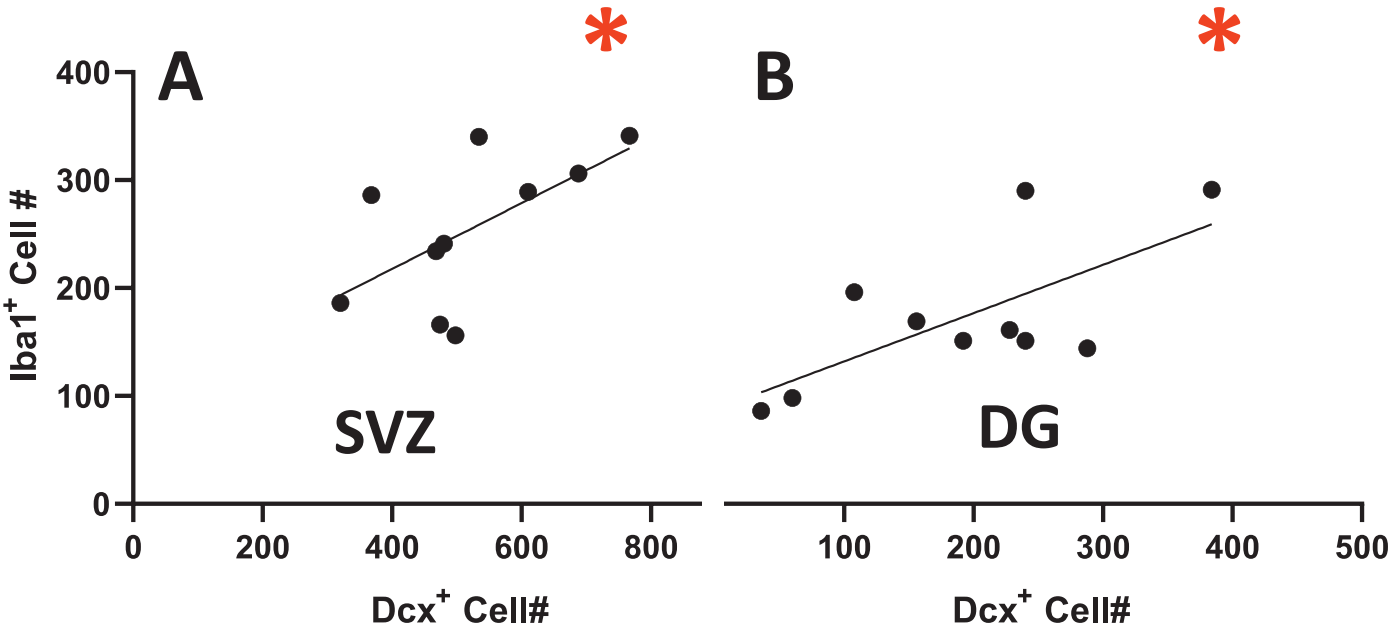


**FIG. 6.** Correlation plots of Iba1 vs. DCX cell numbers in the SVZ and DG. Simple linear regressions were used to test if Iba1$^+$ cell number significantly predicted DCX$^+$ cell number in the SVZ (panel A) and the DG (panel B); the SVZ data was squared transformed prior to linear regression procedure. The overall regressions were statistically significant for the SVZ [$R^2 = 0.427$, $F(1,8) = 5.951$, $P = 0.041$] and the DG [$R^2 = 0.472$, $F(1,8) = 7.151$, $P = 0.028$].

striatum, SVZ, and DG of individual rats. Microglia activation was significantly elevated in the SVZ and the DG, both important sites of neurogenesis. Our data indicate that the number of immature neurons (DCX$^+$) in the DG hilus was significantly elevated and positively correlated with microglial cell number in irradiated rats. Typically, DCX$^+$ cells are not usually found in the DG hilus. The features of the DCX$^+$ cells located in the DG in the current study were consistent with hilar ectopic granule cells (hEGC). Notably, these cells have morphological and physiological similarities to normal granule cells located in the GCL layer (*64*). The space radiation-induced appearance of hEGC within the hilus may be responsible, in part, for the widely reported loss of hippocampal function post-space radiation exposure. The presence of a small (<5% of all granular cells) but hyperexcitable population of neurons in the hilus is sufficient to impair DG-dependent functions (*65*) and disrupt the functionality of hippocampal circuitry (*66*). In addition to the behavioral issues that may arise due to a space radiation-induced increase of DCX$^+$ cells in the DG hilus after exposure, there may be an elevated risk of developing brain cancer, given that elevated DCX$^+$ levels may be predictive of neuroblastoma risk (*67*). Microglia are known to release important trophic factors, such as BDNF, NGF1 and IGF (*68*). One study infused BDNF into the hippocampus which increased the number of ectopically located neurons (*69*). Therefore, the increase in microglia could be one mechanism responsible for the elevated immature neurons in the present study. While neurotrophic levels were not measured in the current study,

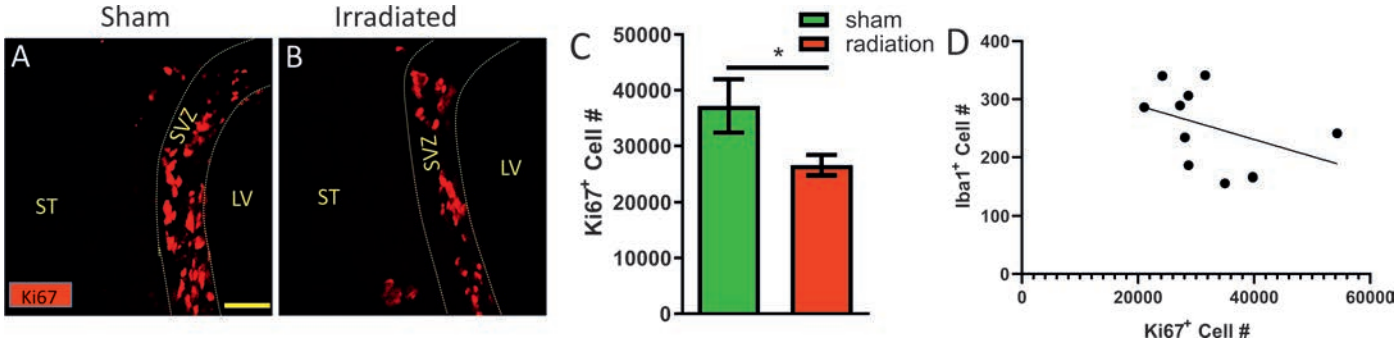


**FIG. 7.** [28]Silicon radiation decreased proliferative (Ki67$^+$) cells in the SVZ. Panels A and B: Representative Ki67 immunofluorescence staining showing cell proliferation confining to the SVZ. Panel C: Histogram of Ki67$^+$ cell count in the SVZ. Panel D: Correlation plot of Iba1 vs. Ki67 cell numbers in the SVZ. Simple linear regressions were used to test if Iba1$^+$ cell number significantly predicted Ki67$^+$ cell number. The overall regression was not statistically significant [$R^2 = 0.163$, $F(1,8) = 1.555$, $P = 0.248$]. Yellow dashed lines outline the SVZ. Scale bar = 50 μm. Student's t test performed on transformed data, * denotes $P \leq 0.05$. Error bars = SEM. ST = striatum, LV = lateral ventricle.

**TABLE 3**
**Summary of Results**

| | SVZ | Striatum | DG |
|---|---|---|---|
| Iba1 cell number | ↑ | N/A | ∅ |
| Iba1 morphology | ∅ | Activated | Activated |
| DCX cell count | ∅ | N/A | ↑ |
| Ki67 cell count | ↓ | N/A | N/A |

another group found exposure to space radiation was accompanied by microglial activation and an increased level of the neurotrophic factor BDNF in the CNS (*70, 71*).

In the current study, low doses of $^{28}$Si radiation resulted in a significant decrease in proliferative cells (Ki67$^+$) in the SVZ. This decrease in SVZ proliferation may be both a result of a defect in the proliferative capacity of the neural stem cell pool and changes to the neurogenic microenvironment as previously observed in the DG in response to X rays (*44*), $^{56}$Fe (*72*) and $^{28}$Si (*42*). In addition to the role that suppressed neurogenesis may have on cognitive performance, the persistent suppression of neurogenesis may also have wide ramifications for other functions, including sensorimotor. Neurogenesis is thought to be an important contributor to functional recovery after brain trauma (*73, 74*). Thus, it is possible that astronauts may have a reduced ability to cope with future CNS trauma or a neurodegenerative disease, thereby impacting astronauts' life long after the completion of their deep space mission.

Overall, this study demonstrated that a single low dose of radiation from a single ion ($^{28}$Si) results in persistent cellular effects (as examined at five months postirradiation) that could have immediate (behavioral) and long-term (neurodegenerative disease) neurological consequences. While the sample size was small and no cytokine expression was directly measured, the persistent microglial activation in areas of the striatum, SVZ, and DG may be a potential mechanism for cognitive and sensorimotor deficits associated with space radiation exposure. Such changes may be the driving force for the altered neurogenesis within the SVZ and DG, including the presence of hilar ectopic neurons within the DG. While exposure to space radiation has a marked effect on microglia, the long-term consequences of space radiation-induced activation of microglia needs to be investigated further to provide a more complete view of the impact of neuroinflammation on astronauts returning from deep space missions.

## SUPPLEMENTARY MATERIALS

Supplementary Fig. S1. Microglia populations exhibited heterogeneity in morphology and were significantly different in the hilus, SVZ and striatum in control animals. Panels A-D: Violin plots of Iba1$^+$ microglia cells' area, perimeter, circularity, and ramification indexes respectively. One-way ANOVA, Tukey HSD post hoc test, *denotes $P \leq 0.05$, **denotes $P \leq 0.005$, ***denotes $P \leq 0.0005$.

Supplementary Fig. S2. $^{28}$Silicon radiation significantly changed Iba1 morphology in the striatum and DG. Panels A–C and A'–C'. Plots of circularity and ramification of Iba1$^+$ cells in each individual rat used in this study are shown. Each dot represents a single Iba1$^+$ cell.

## ACKNOWLEDGMENTS

We thank the Office of Academic Affiliations, VA Advanced Fellowship in Polytrauma/Traumatic Brain Injury Rehabilitation; Department of Veterans Affairs and funding from NASA grant award NNX14AE73G.

Received: November 4, 2021; accepted: March 17, 2022; published online: April 4, 2022

## REFERENCES

1. Cucinotta FA, Alp M, Sulzman FM, Wang M. Space radiation risks to the central nervous system. Life Sci Space Res. 2014;2:54-69.
2. Slaba TC, Blattnig SR, Norbury JW, Rusek A, La Tessa C. Reference field specification and preliminary beam selection strategy for accelerator-based GCR simulation. Life Sci Space Res (Amst). 2016;8:52-67.
3. Britten RA, Duncan VD, Fesshaye A, Rudobeck E, Nelson GA, Vlkolinsky R. Altered cognitive flexibility and synaptic plasticity in the rat prefrontal cortex after exposure to low (</ = 15 cGy) doses of (28)Si radiation. Radiat Res. 2020; 193(3):223-35.
4. Blackwell AA, Schell BD, Osterlund Oltmanns JR, Whishaw IQ, Ton ST, Adamczyk NS, et al. Skilled movement and posture deficits in rat string-pulling behavior following low dose space radiation ((28)Si) exposure. Behav Brain Res. 2021; 400:113010.
5. Kartje G, Schulz M, Lopez-Yunez A, Schnell L, Schwab M. Corticostriatal plasticity is restricted by myelin-associated neurite growth inhibitors in the adult rat. Ann Neurology. 1999; 45(6):778-86.
6. Rogers RD, Baunez C, Everitt BJ, Robbins TW. Lesions of the medial and lateral striatum in the rat produce differential deficits in attentional performance. Behavioral Neurosci. 2001; 115(4):799.
7. Kalueff AV, Stewart AM, Song C, Berridge KC, Graybiel AM, Fentress JC. Neurobiology of rodent self-grooming and its value for translational neuroscience. Nat Rev Neurosci. 2016; 17(1):45-59.
8. O'Doherty J, Dayan P, Schultz J, Deichmann R, Friston K, Dolan RJ. Dissociable roles of ventral and dorsal striatum in instrumental conditioning. Science. 2004; 304(5669):452-4.
9. Tricomi EM, Delgado MR, Fiez JA. Modulation of caudate activity by action contingency. Neuron. 2004; 41(2):281-92.
10. Dorfman HM, Tomov MS, Cheung B, Clarke D, Gershman SJ, Hughes BL. Causal inference gates corticostriatal learning. J Neurosci. 2021; 41(32):6892-904.
11. Bellone JA, Rudobeck E, Hartman RE, Szucs A, Vlkolinsky R. A single low dose of proton radiation induces long-term behavioral and electrophysiological changes in mice. Radiat Res. 2015; 184(2):193-202.
12. Britten RA, Davis LK, Jewell JS, Miller VD, Hadley MM, Sanford LD, et al. Exposure to mission relevant doses of 1 GeV/Nucleon (56)Fe particles leads to impairment of attentional set-shifting performance in socially mature rats. Radiat Res. 2014; 182(3):292-8.
13. Machida M, Lonart G, Britten RA. Low (60 cGy) doses of 56Fe HZE-particle radiation lead to a persistent reduction in the glutamatergic readily releasable pool in rat hippocampal synaptosomes. Radiat Res. 2010; 174(5):618-23.
14. Marty VN, Vlkolinsky R, Minassian N, Cohen T, Nelson GA,

Spigelman I. Radiation-induced alterations in synaptic neurotransmission of dentate granule cells depend on the dose and species of charged particles. Radiat Res. 2014; 182(6):653-65.

15. Rudobeck E, Nelson GA, Sokolova IV, Vlkolinský R. 28Silicon radiation impairs neuronal output in CA1 neurons of mouse ventral hippocampus without altering dendritic excitability. Radiat Res. 2014; 181(4):407-15.
16. Sokolova IV, Schneider CJ, Bezaire M, Soltesz I, Vlkolinsky R, Nelson GA. Proton radiation alters intrinsic and synaptic properties of CA1 pyramidal neurons of the mouse hippocampus. Radiat Res. 2015; 183(2):208-18.
17. Parihar VK, Maroso M, Syage A, Allen BD, Angulo MC, Soltesz I, et al. Persistent nature of alterations in cognition and neuronal circuit excitability after exposure to simulated cosmic radiation in mice. Exp Neurol. 2018; 305:44-55.
18. Klein PM, Parihar VK, Szabo GG, Zoldi M, Angulo MC, Allen BD, et al. Detrimental impacts of mixed-ion radiation on nervous system function. Neurobiol Dis. 2021; 151:105252.
19. Perea G, Araque A. Glial calcium signaling and neuron–glia communication. Cell calcium. 2005; 38(3-4):375-82.
20. Fields RD, Stevens-Graham B. New insights into neuron-glia communication. Science. 2002; 298(5593):556-62.
21. Vezzani A, Ravizza T, Balosso S, Aronica E. Glia as a source of cytokines: implications for neuronal excitability and survival. Epilepsia. 2008; 49:24-32.
22. Devinsky O, Vezzani A, Najjar S, De Lanerolle NC, Rogawski MA. Glia and epilepsy: excitability and inflammation. Trends Neurosci. 2013; 36(3):174-84.
23. Bachiller S, Jimenez-Ferrer I, Paulus A, Yang Y, Swanberg M, Deierborg T, et al. Microglia in neurological diseases: a road map to brain-disease dependent-inflammatory response. Front Cell Neurosci. 2018; 12:488.
24. Kwon HS, Koh SH. Neuroinflammation in neurodegenerative disorders: the roles of microglia and astrocytes. Transl Neurodegener. 2020; 9(1):42.
25. Leng F, Edison P. Neuroinflammation and microglial activation in Alzheimer disease: where do we go from here? Nat Rev Neurol. 2021; 17(3):157-72.
26. Otani K, Shichita T. Cerebral sterile inflammation in neurodegenerative diseases. Inflamm Regen. 2020; 40(1):28.
27. Streit WJ, Khoshbouei H, Bechmann I. The role of microglia in sporadic Alzheimer's disease. J Alzheimers Dis. 2021; 79:961-68.
28. Barros C, Fernandes A. Linking cognitive impairment to neuroinflammation in multiple sclerosis using neuroimaging tools. Mult Scler Relat Disord. 2020:102622.
29. Acharya MM, Green KN, Allen BD, Najafi AR, Syage A, Minasyan H, et al. Elimination of microglia improves cognitive function following cranial irradiation. Sci Rep. 2016; 6(1):31545.
30. Krukowski K, Feng X, Paladini MS, Chou A, Sacramento K, Grue K, et al. Temporary microglia-depletion after cosmic radiation modifies phagocytic activity and prevents cognitive deficits. Sci Rep. 2018; 8(1):1-13.
31. Allen BD, Syage AR, Maroso M, Baddour AAD, Luong V, Minasyan H, et al. Mitigation of helium irradiation-induced brain injury by microglia depletion. J Neuroinflammat. 2020; 17(1):159.
32. Britten RA, Wellman LL, Sanford LD. Progressive increase in the complexity and translatability of rodent testing to assess space-radiation induced cognitive impairment. Neurosci Biobehav Rev. 2021; 126:159-74.
33. Hong S, Stevens B. Microglia: Phagocytosing to clear, sculpt, and eliminate. Dev Cell. 2016; 38(2):126-8.
34. Hong S, Beja-Glasser VF, Nfonoyim BM, Frouin A, Li S, Ramakrishnan S, et al. Complement and microglia mediate early synapse loss in Alzheimer mouse models. Science. 2016; 352(6286):712-6.
35. Sierra A, Encinas JM, Deudero JJ, Chancey JH, Enikolopov G, Overstreet-Wadiche LS, et al. Microglia shape adult hippocampal neurogenesis through apoptosis-coupled phagocytosis. Cell Stem Cell. 2010; 7(4):483-95.
36. Diaz-Aparicio I, Paris I, Sierra-Torre V, Plaza-Zabala A, Rodríguez-Iglesias N, Márquez-Ropero M, et al. Microglia actively remodel adult hippocampal neurogenesis through the phagocytosis secretome. J Neurosci. 2020; 40(7):1453-82.
37. Walton NM, Sutter BM, Laywell ED, Levkoff LH, Kearns SM, Marshall GP, 2nd, et al. Microglia instruct subventricular zone neurogenesis. Glia. 2006; 54(8):815-25.
38. Rodríguez-Iglesias N, Sierra A, Valero J. Rewiring of memory circuits: connecting adult newborn neurons with the help of microglia. Front Cell Dev Biol. 2019; 7:24.
39. Vukojicic A, Delestree N, Fletcher EV, Pagiazitis JG, Sankaranarayanan S, Yednock TA, et al. The classical complement pathway mediates microglia-dependent remodeling of spinal motor circuits during development and in SMA. Cell Rep. 2019; 29(10):3087-100 e7.
40. Chamera K, Kotarska K, Szuster-Gluszczak M, Trojan E, Skorkowska A, Pomierny B, et al. The prenatal challenge with lipopolysaccharide and polyinosinic:polycytidylic acid disrupts CX3CL1-CX3CR1 and CD200-CD200R signalling in the brains of male rat offspring: a link to schizophrenia-like behaviours. J Neuroinflammation. 2020; 17(1):247.
41. Chamera K, Trojan E, Szuster-Gluszczak M, Basta-Kaim A. The potential role of dysfunctions in neuron-microglia communication in the pathogenesis of brain disorders. Curr Neuropharmacol. 2020; 18(5):408-30.
42. Whoolery CW, Walker AK, Richardson DR, Lucero MJ, Reynolds RP, Beddow DH, et al. Whole-body exposure to (28)Si-radiation dose-dependently disrupts dentate gyrus neurogenesis and proliferation in the short term and new neuron survival and contextual fear conditioning in the long term. Radiat Res. 2017; 188(5):532-51.
43. Rola R, Sarkissian V, Obenaus A, Nelson GA, Otsuka S, Limoli CL, Fike JR. High-LET radiation induces inflammation and persistent changes in markers of hippocampal neurogenesis. Radiat Res. 2005; 164(4):556-60.
44. Monje ML, Mizumatsu S, Fike JR, Palmer TD. Irradiation induces neural precursor-cell dysfunction. Nat Med. 2002; 8(9):955-62.
45. Krukowski K, Grue K, Frias ES, Pietrykowski J, Jones T, Nelson G, et al. Female mice are protected from space radiation-induced maladaptive responses. Brain Behav Immun. 2018; 74:106-20.
46. Belcher EK, Sweet TB, Karaahmet B, Dionisio-Santos DA, Owlett LD, Leffler KA, et al. Cranial irradiation acutely and persistently impairs injury-induced microglial proliferation. Brain Behav Immun Health. 2020; 4:100057.
47. Ton ST, Adamczyk NS, Gerling JP, Vaagenes IC, Wu JY, Hsu K, et al. Dentate gyrus proliferative responses after traumatic brain injury and binge alcohol in adult rats. Neurosci Insights. 2020; 15:2633105520968904.
48. Ton ST, Tsai SY, Vaagenes IC, Glavin K, Wu J, Hsu J, et al. Subventricular zone neural precursor cell responses after traumatic brain injury and binge alcohol in male rats. J Neurosci Res. 2019; 97(5):554-67.
49. Iwano T, Masuda A, Kiyonari H, Enomoto H, Matsuzaki F. Prox1 postmitotically defines dentate gyrus cells by specifying granule cell identity over CA3 pyramidal cell fate in the hippocampus. Development. 2012; 139(16):3051-62.
50. Joseph J, Hunt W, Rabin B, Dalton T. Possible ''accelerated striatal aging'' induced by 56Fe heavy-particle irradiation: Implications for manned space flights. Radiat Res. 1992; 130(1):88-93.
51. Rabin BM, Hunt WA, Joseph JA. An assessment of the behavioral toxicity of high-energy iron particles compared to other qualities of radiation. Radiat Res. 1989; 119(1):113-22.
52. Rabin BM, Hunt WA, Joseph JA, Dalton TK, Kandasamy SB. Relationship between linear energy transfer and behavioral toxicity

in rats following exposure to protons and heavy particles. Radiat Res. 1991; 128(2):216-21.

53. Mange A, Cao Y, Zhang S, Hienz RD, Davis CM. Whole-body oxygen ((16)O) ion-exposure-induced impairments in social odor recognition memory in rats are dose and time dependent. Radiat Res. 2018; 189(3):292-9.

54. Jones CB, Mange A, Granata L, Johnson B, Hienz RD, Davis CM. Short and long-term changes in social odor recognition and plasma cytokine levels following oxygen ((16)O) ion radiation exposure. Int J Mol Sci. 2019; 20(2):339.

55. Kiffer F, Boerma M, Allen A. Behavioral effects of space radiation: A comprehensive review of animal studies. Life Sci Space Res (Amst). 2019; 21:1-21.

56. Burket JA, Matar M, Fesshaye A, Pickle JC, Britten RA. Exposure to low (</ = 10 cGy) doses of 4He particles leads to increased social withdrawal and loss of executive function performance. Radiat Res. 2021.

57. Torres-Platas SG, Comeau S, Rachalski A, Dal Bo G, Cruceanu C, Turecki G, et al. Morphometric characterization of microglial phenotypes in human cerebral cortex. J Neuroinflamm. 2014; 11(1):1-4.

58. Zanier ER, Fumagalli S, Perego C, Pischiutta F, De Simoni MG. Shape descriptors of the ''never resting'' microglia in three different acute brain injury models in mice. Intensive Care Med Exp. 2015; 3(1):39.

59. Kozlowski C, Weimer RM. An automated method to quantify microglia morphology and application to monitor activation state longitudinally in vivo. PLoS One. 2012; 7(2):e31814.

60. Morrison HW, Filosa JA. A quantitative spatiotemporal analysis of microglia morphology during ischemic stroke and reperfusion. J Neuroinflammation. 2013; 10(1):4.

61. Thored P, Heldmann U, Gomes-Leal W, Gisler R, Darsalia V, Taneera J, et al. Long-term accumulation of microglia with proneurogenic phenotype concomitant with persistent neurogenesis in adult subventricular zone after stroke. Glia. 2009; 57(8):835-49.

62. Jurga AM, Paleczna M, Kuter KZ. Overview of general and discriminating markers of differential microglia phenotypes. Front Cell Neurosci. 2020; 14:198.

63. Rienecker KDA, Paladini MS, Grue K, Krukowski K, Rosi S. Microglia: Ally and enemy in deep space. Neurosci Biobehav Rev. 2021; 126:509-14.

64. Scharfman HE, Goodman JH, Sollas AL. Granule-like neurons at the hilar/CA3 border after status epilepticus and their synchrony with area CA3 pyramidal cells: functional implications of seizure-induced neurogenesis. J Neuro. 2000; 20(16):6144-58.

65. Myers CE, Bermudez-Hernandez K, Scharfman HE. The influence of ectopic migration of granule cells into the hilus on dentate gyrus-CA3 function. PLoS One. 2013; 8(6):e68208.

66. Scharfman HE, Myers CE. Corruption of the dentate gyrus by ''dominant'' granule cells: Implications for dentate gyrus function in health and disease. Neurobiol Learn Mem. 2016; 129:69-82.

67. Ayanlaja AA, Xiong Y, Gao Y, Ji G, Tang C, Abdikani Abdullah Z, et al. Distinct features of doublecortin as a marker of neuronal migration and its implications in cancer cell mobility. Front Mol Neurosci. 2017; 10:199.

68. Cho K, Choi G. Microglia: physiological functions revealed through morphological profiles. Folia Biologica. 2017; 63(3):85.

69. Scharfman H, Goodman J, Macleod A, Phaxni S, Antonelli C, Croll S. Increased neurogenesis and the ectopic granule cells after intrahippocampal BDNF infusion in adult rats. Exp Neurol. 2005; 192(2):348-56.

70. Raber J, Yamazaki J, Torres ERS, Kirchoff N, Stagaman K, Sharpton T, et al. Combined effects of three high-energy charged particle beams important for space flight on brain, behavioral and cognitive endpoints in B6D2F1 female and male mice. Front Physiol. 2019; 10:179.

71. Raber J, Fuentes Anaya A, Torres ERS, Lee J, Boutros S, Grygoryev D, et al. Effects of six sequential charged particle beams on behavioral and cognitive performance in B6D2F1 female and male mice. Front Physiol. 2020; 11:959.

72. Sweet TB, Hurley SD, Wu MD, Olschowka JA, Williams JP, O'Banion MK. Neurogenic effects of low-dose whole-body HZE (Fe) ion and gamma irradiation. Radiat Res. 2016; 186(6):614-23.

73. Shiromoto T, Okabe N, Lu F, Maruyama-Nakamura E, Himi N, Narita K, et al. The role of endogenous neurogenesis in functional recovery and motor map reorganization induced by rehabilitative therapy after stroke in rats. J Str Cerebrovasc Dis. 2017; 26(2):260-72.

74. Zhao C, Deng W, Gage FH. Mechanisms and functional implications of adult neurogenesis. Cell. 2008; 132(4):645-60.